Tailoring polyamide rejection layer with aqueous carbonate chemistry for enhanced membrane separation: Mechanistic insights, chemistry-structure-property relationship, and environmental implications

Lu Elfa Peng,[†] Zhikan Yao,[‡] Xin Liu,[§] Baolin Deng,[§,∥] Hao Guo,*[,†] Chuyang Y. Tang*[,†,⊥,#]

[†]Department of Civil Engineering, The University of Hong Kong, Pokfulam, Hong Kong SAR, China.

[‡]College of Chemical and Biological Engineering, Zhejiang University, Hangzhou, 310027, China

[§]School of Environmental Science and Engineering, Southern University of Science and Technology, Shenzhen, 518005, China.

[∥]Department of Civil and Environmental Engineering, University of Missouri, Columbia, Missouri, 65211, United States

[⊥]UNESCO Centre for Membrane Science and Technology, School of Chemical Engineering, University of New South Wales, Sydney, New South Wales, 2052, Australia

[#]UNSW Water Research Centre, School of Civil and Environmental Engineering, University of New South Wales, Sydney, New South Wales, 2052, Australia

[*]Corresponding Authors:

Hao Guo, guohao7@hku.hk, +852 28578470

Chuyang Y. Tang, tangc@hku.hk, +852 28591976

28 **TABLE OF CONTENTS**

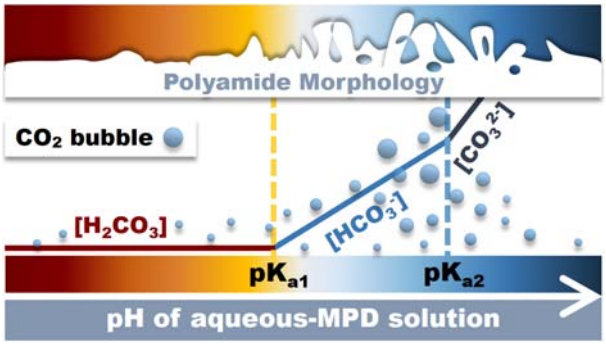

29

30

ABSTRACT

Surface roughness and the associated nanosized voids inside the roughness structures have great influence on the separation performance of thin film composite polyamide reverse osmosis (RO) membranes. Inspired by the recent findings that these voids are formed due to the degassing of CO_2 nanobubbles during interfacial polymerization, we systematically investigated the role of carbonate chemistry, particularly the solubility of CO_2, in the aqueous *m*-phenylenediamine (MPD) solution for the first time. "Ridge-and-valley" roughness features were obtained when the pH of the MPD solution was between the two acidity constants of the carbonate system (i.e. $6.3 \leq pH \leq 10.3$), under which condition HCO_3^- dominates over the other carbonate species. Increasing pH over this range led to both increased water permeability and better rejection of various solutes, thanks to the simultaneously enhanced effective filtration area and crosslinking degree of the polyamide layer. Further increase of pH to 12.5 resulted in more disparate rejection results due to membrane hydrolysis: rejection of neural solutes (B and As(III)) was compromised whereas that of charged solutes (NaCl and As(V)) was maintained. The mechanistic insights gained in the current study reveal the critical need to design RO membranes directly for end applications based on first principles.

INTRODUCTION

Membrane-based desalination and water reuse rely on thin film composite (TFC) reverse osmosis (RO) membranes,[1, 2] whose separation performance is largely determined by the structure and morphology of a thin polyamide rejection film.[3, 4] A typical polyamide film has a rough structure consisting of random protuberances that are often known as "ridge-and-valley" structures.[5-7] Recent microscopic characterization has visualized nano-sized hollow voids within these protuberances,[8-11] which are believed to greatly enhance membrane permeability.[6, 9-13] Despite the increased number of studies investigating membrane surface roughness formation under various fabrication conditions,[13-19] the formation mechanism of nanovoids during the interfacial polymerization (IP) of polyamide remains poorly understood.

During a typical IP reaction, an aqueous solution of *m*-phenylenediamine (MPD) reacts with an organic solution of trimesoyl chloride (TMC) at the water/organic interface. Some earlier studies hypothesized that nanovoids are generated by the diffusion of aqueous MPD droplets into the organic solution, forming polyamide at the droplet/organic interface and leaving pores within.[20, 21] Others believe that these nanovoids are caused by interfacial instability.[22, 23] However, the recent studies by Ma et al. [24, 25] suggest that these nanovoids were primarily formed by the release of carbon dioxide (CO_2) nano-bubbles. During the IP reaction, acid and heat are generated (Figure 1A), which promotes the degas of CO_2 from the aqueous solution. This nanofoaming theory offers new opportunities to tailor the polyamide rejection layer for enhanced membrane separation.[24-26]

Presumably, the release of CO_2 nanobubbles can be greatly affected by the solubility of the gas in the aqueous phase. Therefore, we hypothesize that the aquatic chemistry of the MPD solution can play a major role in shaping the morphology of the polyamide rejection layer. In particular, the solubility of CO_2 can increase by several orders of magnitude at higher pH (Figure 1B), which prompts us to investigate the fundamental role of pH during the formation of the polyamide rejection layer. Despite the many existing studies involving IP reactions at different pH,[27-29] the critical role of aqueous carbonate chemistry (particularly CO_2 solubility) and its impact on the morphology and separation properties of polyamide membranes have not yet been systematically studied.

Here we performed detailed characterization of polyamide membranes formed over a wide range of pH to reveal the underlying chemistry-structure-property relationship. We further investigated the rejection of selected trace contaminants (boron and arsenic) in addition to water permeability and NaCl rejection to resolve the major mechanisms in polyamide formation. The current study provides a fundamental framework for in-depth understanding of the role of aqueous chemistry during the interfacial polymerization of TFC RO membranes, which has important implications for tailored membrane development for desalination and water reuse applications.

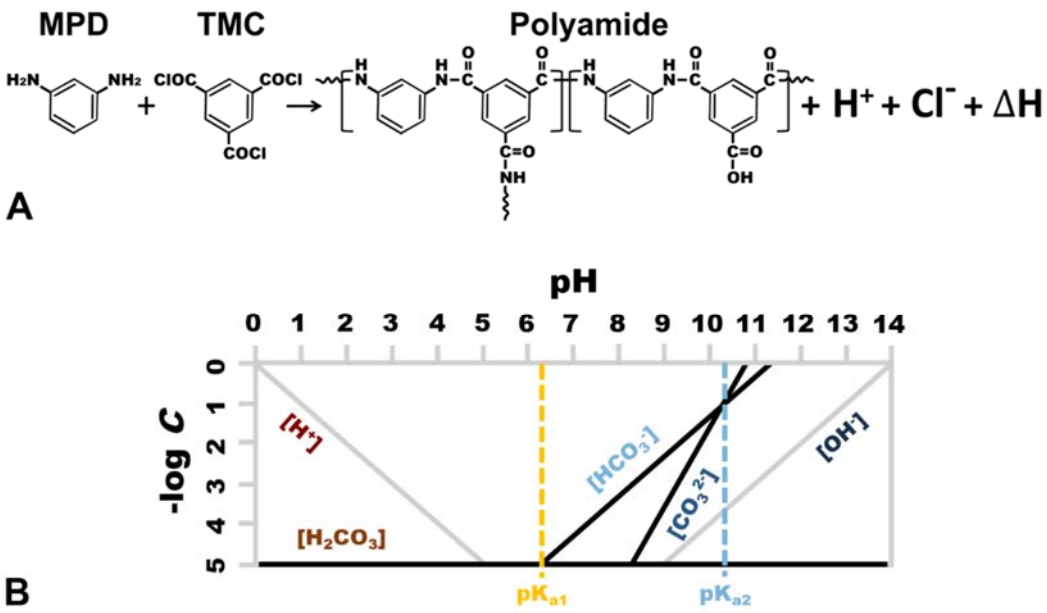

Figure 1. (A) The reaction involved in the interfacial polymerization of MPD and TMC, which generates hydrochloric acid ($H^+ + Cl^-$) and heat (ΔH). (B) The effect of pH on the solubility of CO_2.[30] To obtain the concentration *C* of the dissolved species ($[H^+]$, $[H_2CO_3]$, $[HCO_3^-]$, $[CO_3^{2-}]$ and $[OH^-]$), it is assumed that the aqueous solution is in equilibrium with the ambient atmospheric CO_2.[30] The total dissolved CO_2 concentration is the sum of $[H_2CO_3]$, $[HCO_3^-]$, and $[CO_3^{2-}]$.

MATERIALS AND METHODS

Chemicals. Polysulfone (PSf, Mw~35,000, Sigma-Aldrich) and dimethylformamide (DMF, anhydrous 99.8%, Sigma-Aldrich) were used to prepare the porous substrate. *m*-phenylenediamine (MPD, 99%, Sigma-Aldrich), trimesoyl chloride (TMC, 98%, Sigma-Aldrich), and n-hexane (HPLC grade, ≥95%, Sigma-Aldrich) were used in interfacial polymerization as the aqueous phase monomer, organic phase monomer, and organic phase solvent, respectively. Sodium hydroxide (NaOH, Dieckmann) and hydrochloric acid (HCl, 37%, VWR) were used for pH adjustment. Sodium chloride (NaCl, Dieckmann), boric acid ($B(OH)_3$, Dieckmann), sodium arsenate dibasic

heptahydrate ($HAsNa_2O_4 \cdot 7H_2O$, Sigma-Aldrich), and arsenic (III) oxide (As_2O_3, ≥99.0%, Sigma-Aldrich) were used for membrane rejection tests.

Membrane fabrication. The PSf substrate was fabricated using a non-solvent induced phase separation method.[31] Briefly, a 15 wt% PSf dissolved in DMF was casted onto a clean glass plate with an automatic film applicator (Elcometer 4340, Elcometer, gate height of 150 μm). The PSf substrate, after being coagulated in deionized (DI) water at room temperature (~ 25 ˚C), was thoroughly rinsed and soaked with DI water before further using.

Interfacial polymerization was performed on the PSf substrate using 1 wt.% aqueous MPD solution and 0.1 wt.% of TMC in hexane. The MPD solution without any pH adjustment has a solution pH of approximately 9.3. In order to investigate the role of pH on the formation of polyamide layer, additional aqueous solution pH of 4.0, 5.0, 6.3, 10.3, and 12.5 (by the addition of HCl or NaOH solution) were included, where pH 6.3 and 10.3 correspond to the two acidity constants pKa_1 and pKa_2 of the carbonate system (Figure 1B). To perform the IP reaction, the PSf substrate was first soaked in the aqueous MPD solution for 2 min. Excess MPD solution was gently removed by a rubber roller. The MPD impregnated PSf substrate was then soaked in the TMC/hexane solution for 1 min to form the polyamide rejection layer. The formed polyamide membrane was rinsed by hexane and kept in 50 ˚C Milli-Q water for 10 min for further polymerization. The prepared membranes were named as TFC-pHX, where X is the pH value of the corresponding MPD solution.

Membrane characterization. Unless specified elsewhere, all membrane samples were freeze vacuum-dried before characterization. Field-emission scanning electron microscopy (FE-SEM, S-4800, Hitachi) was used to characterize membrane surface morphology. Dried membrane samples were sputter-coated with a thin gold layer followed by an SEM scanning operated at an accelerating voltage of 5.0 kV. Transmission electron microscopy (TEM, CM100, Philips) was used to resolve membrane cross section structure at an accelerating voltage of 100 kV. Atomic force microscopy (AFM, MFP-3D, Asylum Research) was used to determine membrane surface roughness with a scanning range of 5.0 × 5.0 μm^2. X-ray photoelectron spectroscopy (XPS, Thermo Fishier Scientific) was employed to analyze the elemental composition of membrane surface. The analysis was performed using an X-ray source of Al Kα gun with a spectra range of 0-1350 eV. The obtained atomic percent of O and N were used to calculate the ratio of oxygen to nitrogen (O/N) of the polyamide layer, which can be further used to determine its crosslinking degree (Supporting Information S1). Zeta potential analyzer (EKA, SurPASS 3, Anton Paar) were applied to measure membrane surface charge in a 1.0 mM potassium chloride background solution with a pH range of 3.0~10.0. Attenuated total reflectance Fourier transform infrared spectroscopy (ATR-FTIR, Nicolet iS5, Thermo Fisher Scientific) was used to scan functional groups on membrane surface over a wavenumber range of 650-4000 cm^{-1}.

Membrane separation performance. Membrane separation performance including water flux and solutes rejection were tested using a laboratory-scale cross-flow RO filtration system (Supporting Information S2).[32] A membrane coupon was loaded in a stainless steel cell with an effective filtration area of 12.0 cm^2 and was pre-compacted at 17.0 bar for 2 h with a cross-flow velocity of 22.4 cm/s under room temperature (~

25 ˚C). The permeate samples were then collected at 15.5 bar to measure water flux and solute rejection. The water flux and permeability were calculated by:[33]

$$J_v = \frac{\Delta m}{\Delta t \times a \times \rho} \quad (1)$$

$$A = \frac{J_v}{\Delta P - \Delta \pi} \quad (2)$$

where J_v (L m^{-2} h^{-1}) is the water flux, Δm (kg) is the mass of permeate over a time interval of Δt (h), a (m^2) is the effective membrane area, ρ is the density of water (i.e., 1.0 kg L^{-1}), A (L m^{-2} h^{-1} bar^{-1}) is the water permeability coefficient, ΔP (bar) is the transmembrane pressure, and $\Delta \pi$ (bar) is the osmotic pressure across the membranes.

Salt rejection was tested using 2000 ppm NaCl as feed solution. The solution conductivity was measured by a portable conductivity meter (Ultrameter II, Myron L), which can be subsequently converted to the NaCl concentration in the feed and permeate solution (i.e., C_f and C_p, respectively).[34] NaCl rejection (R) and permeability (B) were calculated by:[35]

$$R = \frac{C_f - C_p}{C_f} \times 100\% \quad (3)$$

$$B = (\frac{1}{R} - 1) \times J_v \quad (4)$$

The rejection of trace contaminants were investigated using a feed solution containing 5 ppm boron, 1 ppm As(III), and/or 1 ppm As(V). The concentration of boron and arsenic were determined by an inductively coupled plasma spectrometry (ICP-MS, Agilent 7900).

RESULTS AND DISCUSSION

Effect of pH on membrane morphology and structure

TFC-pH4.0 had a relatively flat surface without the typical "ridge-and-valley" appearance (Figure 2A1) for polyamide RO membranes, which is in direct contrast to the "ridge-and-valley" morphology for membranes formed at pH ≥ 6.3 (Figure 2A3-6). Furthermore, TFC-pH5.0 (Figure 2A2) showed a transitional appearance between the two distinctively different surface morphologies. These results reveal the critical role of aqueous carbonate chemistry on the structure of polyamide membranes. The low solubility of CO_2 at pH ≤ pK_{a1} (i.e. pH 6.3) likely reduces the formation of CO_2 nanobubbles during the IP process much like what occurs for degassing the amine solutions[24] or varying sodium bicarbonate concentration,[25] and thus results in a relatively flat surface of TFC-pH4.0. The CO_2 solubility is greatly enhanced at pH ≥ pK_{a1} as evident from the significantly increased concentration of HCO_3^-. During the IP reaction, HCO_3^- accepts the proton generated (Eq. 5 and Figure 1A), which releases CO_2 gas bubbles under the influence of IP heating:

$$HCO_3^- + H^+ \rightarrow H_2CO_3 \xrightarrow{\text{Heat}} H_2O + CO_2 \uparrow \quad (5)$$

The "ridge-and-valley" structure (Figure 2A3 ~ 2A6) obtained at pH ≥ pK_{a1} is likely caused by the enhanced CO_2 release. According to Ma et al.,[24] the release of CO_2 nanobubbles promotes the formation of roughness features. In their control experiment, these authors degassed the MPD solution to remove the dissolved CO_2 before the interfacial polymerization, and the resulting polyamide membrane did not show the "ridge-and-valley" appearance.

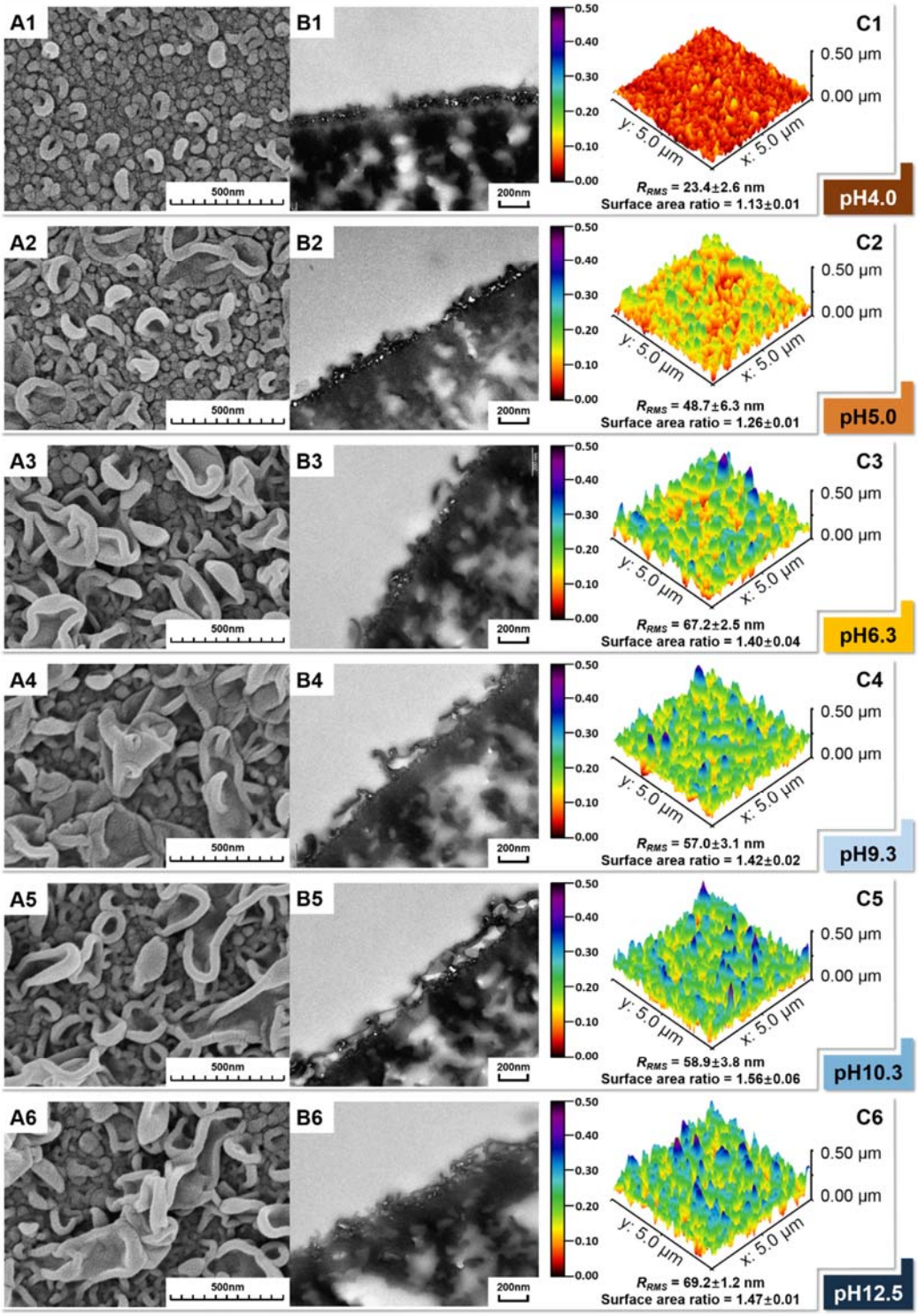

Figure 2. Microscopic characterization of various polyamide TFC membranes. (A) SEM micrographs (top view), (B) TEM micrographs (cross section), and (C) AFM micrographs of top surfaces. R_{RMS} is the root mean square surface roughness. The surface area ratio is defined as the ratio of the measured three-dimensional surface area of the polyamide film to its projected area onto the two-dimensional plane of

the membrane. The projected area is determined by the size of the AFM scan, which was 5.0 × 5.0 μm^2 in the current study.

This explanation is further supported by the TEM and AFM results showing larger roughness features with increased voids size (Figure 2B1-6) and increased surface roughness for membranes formed at pH ≥ pK_{a1} (Figure 2C1-6). However, TFC-pH12.5 showed slightly reduced void contents compared to TFC-pH10.3 (Supporting Information S3), which may be attributed to the predominance of CO_3^{2-} instead of HCO_3^- at pH > pK_{a2} (i.e. pH10.3) in the aqueous solution, in which case the acceptance of a H^+ may not lead to a direct degassing of CO_2:

$$CO_3^{2-} + H^+ \rightarrow HCO_3^- \quad (6)$$

Nevertheless, it is important for the readers to be aware of the inherent limitations of the AFM roughness measurements: (1) some of the valley regions cannot be assessed by the AFM tip due to its finite size,[25] (2) the measurement can be influenced by the curvature of a sample,[24] and (3) the surface roughness is also affected by sample drying.[26]

Effect of pH on cross-linking and surface charge

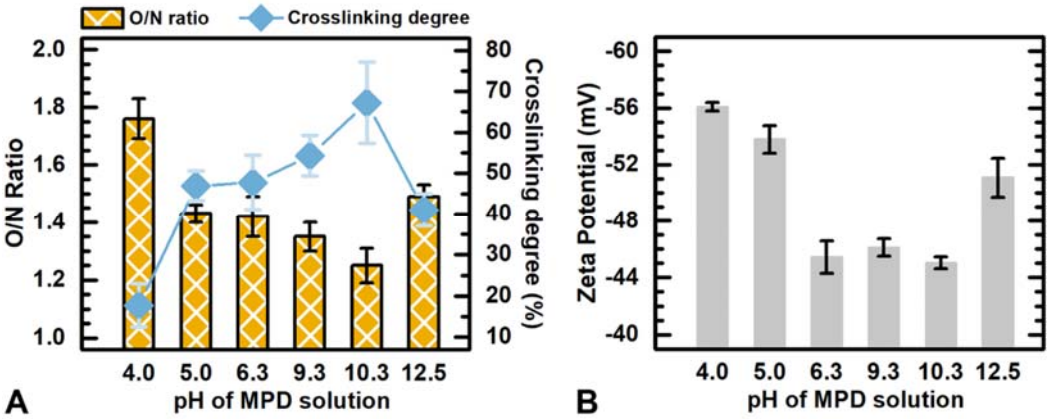

Figure 3. Physicochemical properties of various polyamide TFC membranes. (A) The ratio of oxygen to nitrogen (i.e., the O/N ratio) and the crosslinking degree of various polyamide membranes. The crosslinking degree (n) was calculated from the O/N ratio (r) by: $n = (4-2r)/(1+r)$ in accordance to a previous study[36] (Supporting Information S1). (B) The zeta potential of the TFC membranes. Zeta potential was measured in 1 mM KCl solution. Due to the difficulties in keeping the pH constant under ambient air conditions,[37] the zeta potential value determined was the average of the measured values over the solution pH range of 6.5 to 7.5. Within this pH range, the measured values were relatively constant (see Supporting Information S4). All reported results are the average value from at least three parallel measurements.

The ratio of oxygen to nitrogen (i.e., the O/N ratio, r) obtained from XPS surface analysis decreased from 1.76 ± 0.07 for TFC-pH4.0 to 1.25 ± 0.06 for TFC-pH10.3, corresponding to an improved cross-linking degree from 18 ± 5% to 67 ± 9% (Figure 3A). These values are relatively low compared to typical commercial RO membranes,[38] whose proprietary recipes are optimized in terms of monomer concentrations and additives,[7, 14, 39] which may lead to a higher cross-linking degree.[38] Meanwhile, the membranes formed at pHs between 6.3 to 10.3 were significantly less negatively charged compared to those formed at pH 4.0-5.0 (Figure 3B). These results can be attributed to the more abundant proton acceptor (i.e., OH^-) at higher pH, which could

neutralize H^+, a byproduct generated during IP reaction, to further promote the reaction in the forward direction with enhanced crosslinking degree.[40] At the same time, the reduced carboxyl groups at the increased cross-linking level[12, 14] leads to the less negatively charged membrane surface.

Nevertheless, at the highest pH of the amine solution (pH 12.5), TFC-pH12.5 had a relatively high O/N ratio of 1.49 ± 0.04 with a greatly dropped cross-linking degree of 41 ± 4% as well as more negative surface zeta potential compared to that of TFC-pH10.3. The excess amount of hydroxide (OH^-) at this extremely high pH might compete with MPD monomer to react with TMC as well as to hydrolyze the polyamide layer, which results in reduced cross-linking degree.[27]

Membrane separation performance

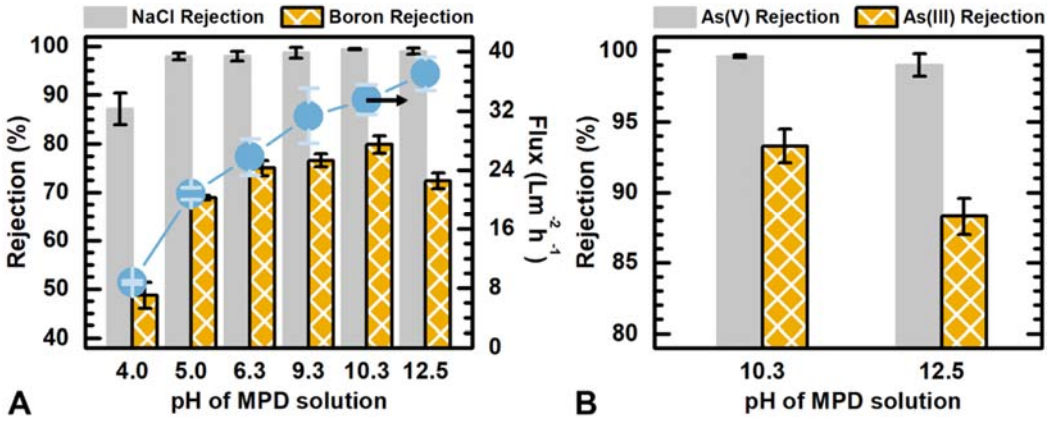

Figure 4. Membrane separation performance including (A) water flux, rejection of NaCl and boron, and (B) rejection of As (III) and As (V) of various membranes. Testing conditions: 2000 ppm NaCl, 5 ppm boron, 1 ppm As (III) and/or 1 ppm As (V) at 15.5 bar with a cross-flow velocity of 22.4 cm/s under room temperature (25 ˚C). All reported results are the average value from at least three parallel measurements.

Membrane water flux was improved via increasing the pH of MPD solution (Figure 4A), which could be attributed to the enhanced membrane surface area ratio and thus greater availability of effective filtration area together with the formation of nanovoids (Figure 2).[13, 16, 24, 41] However, increased surface area ratio alone is not sufficient to explain why TFC-pH12.5 had the highest water flux even though its surface area ratio was lower than that of TFC-pH10.3 (Figure 2C5 and 2C6). The further increase in water flux at the MPD solution pH of 12.5 is likely due to the partial hydrolysis of polyamide. Indeed, amide bonds are known to be hydrolyzed at high pH.[27, 40, 42] Consistently, TFC-pH12.5 had a reduced crosslinking degree compared to TFC-pH10.3 (Figure 3A), which enhances water transport.

Increasing the pH of the MPD solution from 4.0 to 10.3 during IP reaction resulted in enhanced rejection to both NaCl (from 87.2 ± 3.2% to 99.4 ± 0.1%) and boron (from 48.7 ± 2.7% to 79.9 ± 1.8%). Nevertheless, further increasing the pH of the MPD solution to 12.5 led to a reduced rejection of boron (72.4 ± 1.6%), yet without significant impact on NaCl rejection. The rejection of neutrally charged boron is mainly governed by the mechanism of size exclusion, which depends directly on the cross-linking degree of polyamide. High cross-linking degree can enhance the effect of size exclusion and thus improve the rejection of boron by polyamide membrane. On the other hand, the rejection of NaCl is governed by the combined effects of size exclusion and electrostatic interaction. Despite the reduced crosslinking degree of TFC-pH12.5 as a result of membrane hydrolysis, its more negative surface charge helps to maintain the rejection of NaCl thanks to the enhanced Donnan effect.[43-45]

To further confirm the above explanation, we performed additional rejection tests for negatively charged As (V) and neutrally charged As (III) (Figure 4B). TFC-pH12.5 gave a significantly lower rejection of neutral As (III) compared to TFC-pH10.5, whereas no significant change was observed for the rejection of negatively charged As (V) by both membranes. These results are in good agreement with the rejection behavior of boron and NaCl.

IMPLICATIONS

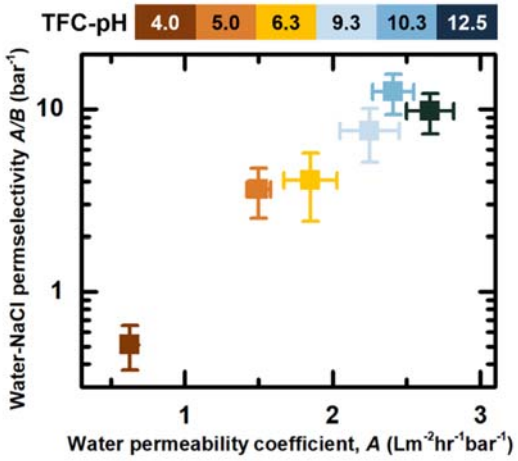

Figure 5. Water-NaCl permselectivity of membranes TFC-pH4.0 ~ TFC-pH12.5. The permselectivity of RO membranes is given by the ratio of water permeability coefficient *A* and solute (NaCl) permeability coefficient *B*.[4]

The current study demonstrates that water chemistry, particularly the classical carbonate chemistry, plays a critical role in shaping the polyamide morphology and turning the polyamide chemistry. Increasing MPD solution pH up to 10.3 resulted in simultaneous enhancement of membrane permselectivity and permeability (Figure 5), thanks to the greater tendency of CO_2 degassing at pH values between the two pKa

values of the carbonate system (6.3 and 10.3, respectively) as well as enhanced cross-linking of the polyamide layer. The membrane chemistry-structure-separation relationship revealed in the current study provides important mechanistic insights, which is critical for designing highly selective and permeable membranes.

Existing RO membrane fabrication literature has largely relied on NaCl rejection (in addition to water permeability) for membrane performance benchmarking and optimization. Nevertheless, many environmental applications require the treatment of trace contaminants that often have critical health implications (e.g., boron in seawater desalination,[46] arsenic in groundwater treatment,[47, 48] and organic micropollutants such as endocrine disruptors and N-nitrosodimethylamine in wastewater reclamation[49, 50]). Membrane makers need to be explicitly aware that a membrane optimized for NaCl rejection and water permeability is not necessarily the best option where neutrally charged trace contaminants are targeted. For example, while TFC-pH12.5 may be considered as the best option for applications targeting primarily salt removal (e.g., brackish water desalination), TFC-pH10.3 is likely more suitable for water reuse application, where higher rejection of neutral contaminants is required in addition to charged solutes. Therefore, future studies need to explore designing RO membranes directly for end applications based on first principles and fundamental mechanisms, in viewing of the deficient current practice of using NaCl rejection as a sole selectivity parameter.

SUPPORTING INFORMATION

S1. Calculation of crosslinking degree; S2. Cross-flow reverse osmosis (RO) filtration system; S3. TEM micrographs for TFC-pH10.3 and TFC-12.5; S4. Zeta potential and XPS results; S5. ATR-FTIR spectra results. This material is available free of charge via the Internet at http://pubs.acs.org.

ACKNOWLEDGMENTS

We thank Ms. Li Wang from Southern University of Science and Technology for providing AFM analysis. We appreciate the State Key Laboratory of Separation Membranes and Membranes Processes of Tianjin Polytechnic University (No.M3-201701) for providing XPS and ATR-FTIR analysis. The School of Biological Science in The University of Hong Kong is appreciated for providing the instrumental analysis platform.

REFERENCES

1. Li, D.; Wang, H. T., Recent developments in reverse osmosis desalination membranes. *J. Mater. Chem.* **2010,** *20*, (22), 4551-4566.
2. Lau, W. J.; Ismail, A. F.; Misdan, N.; Kassim, M. A., A recent progress in thin film composite membrane: A review. *Desalination* **2012,** *287*, 190-199.
3. Jimenez-Solomon, M. F.; Song, Q. L.; Jelfs, K. E.; Munoz-Ibanez, M.; Livingston, A. G., Polymer nanofilms with enhanced microporosity by interfacial polymerization. *Nat. Mater.* **2016,** *15*, (7), 760.
4. Park, H. B.; Kamcev, J.; Robeson, L. M.; Elimelech, M.; Freeman, B. D., Maximizing the right stuff: The trade-off between membrane permeability and selectivity. *Science* **2017,** *356*, (6343), eaab0530.
5. Elimelech, M.; Zhu, X. H.; Childress, A. E.; Hong, S. K., Role of membrane surface morphology in colloidal fouling of cellulose acetate and composite aromatic polyamide reverse osmosis membranes. *J. Membr. Sci.* **1997,** *127*, (1), 101-109.
6. Yan, H.; Miao, X.; Xu, J.; Pan, G.; Zhang, Y.; Shi, Y.; Guo, M.; Liu, Y., The porous structure of the fully-aromatic polyamide film in reverse osmosis membranes. *J. Membr. Sci.* **2015,** *475*, 504-510.
7. Ridgway, H. F.; Orbell, J.; Gray, S., Molecular simulations of polyamide membrane materials used in desalination and water reuse applications: Recent developments and future prospects. *J. Membr. Sci.* **2017,** *524*, 436-448.
8. Pacheco, F. A.; Pinnau, I.; Reinhard, M.; Leckie, J. O., Characterization of isolated polyamide thin films of RO and NF membranes using novel TEM techniques. *J. Membr. Sci.* **2010,** *358*, (1-2), 51-59.
9. Kong, C.; Kanezashi, M.; Yamomoto, T.; Shintani, T.; Tsuru, T., Controlled synthesis of high performance polyamide membrane with thin dense layer for water desalination. *J. Membr. Sci.* **2010,** *362*, (1-2), 76-80.
10. Kong, C.; koushima, A.; Kamada, T.; Shintani, T.; Kanezashi, M.; Yoshioka, T.; Tsuru, T., Enhanced performance of inorganic-polyamide nanocomposite membranes prepared by metal-alkoxide-assisted interfacial polymerization. *J. Membr. Sci.* **2011,** *366*, (1-2), 382-388.
11. Kłosowski, M. M.; McGilvery, C. M.; Li, Y.; Abellan, P.; Ramasse, Q.; Cabral, J. T.; Livingston, A. G.; Porter, A. E., Micro-to nano-scale characterisation of polyamide structures of the SW30HR RO membrane using advanced electron microscopy and stain tracers. *J. Membr. Sci.* **2016,** *520*, 465-476.
12. Kolev, V.; Freger, V., Hydration, porosity and water dynamics in the polyamide layer of reverse osmosis membranes: A molecular dynamics study. *Polymer* **2014,** *55*, (6), 1420-1426.
13. Wong, M. C. Y.; Lin, L.; Coronell, O.; Hoek, E. M. V.; Ramon, G. Z., Impact of liquid-filled voids within the active layer on transport through thin-film composite membranes. *J. Membr. Sci.* **2016,** *500*, 124-135.
14. Ghosh, A. K.; Jeong, B.-H.; Huang, X.; Hoek, E. M. V., Impacts of reaction and curing conditions on polyamide composite reverse osmosis membrane properties. *J. Membr. Sci.* **2008,** *311*, (1-2), 34-45.
15. Kamada, T.; Ohara, T.; Shintani, T.; Tsuru, T., Controlled surface morphology of polyamide membranes via the addition of co-solvent for improved permeate flux. *J. Membr. Sci.* **2014,** *467*, 303-312.
16. Lin, L.; Lopez, R.; Ramon, G. Z.; Coronell, O., Investigating the void structure of the polyamide active layers of thin-film composite membranes. *J. Membr. Sci.* **2016,** *497*, 365-376.
17. Xu, J.; Yan, H.; Zhang, Y.; Pan, G.; Liu, Y., The morphology of fully-aromatic polyamide separation layer and its relationship with separation performance of TFC membranes. *J. Membr. Sci.* **2017,** *541*, 174-188.

18. Jiang, Z.; Karan, S.; Livingston, A. G., Water Transport through Ultrathin Polyamide Nanofilms Used for Reverse Osmosis. *Adv. Mater.* **2018,** *30*, (15), 1705973.
19. Shen, L.; Hung, W.-s.; Zuo, J.; Zhang, X.; Lai, J.-Y.; Wang, Y., High-performance thin-film composite polyamide membranes developed with green ultrasound-assisted interfacial polymerization. *J. Membr. Sci.* **2019,** *570-571*, 112-119.
20. Janssen, L. J. J. M.; Tenijenhuis, K., Encapsulation by Interfacial Polycondensation .1. The Capsule Production and a Model for Wall Growth. *J. Membr. Sci.* **1992,** *65*, (1-2), 59-68.
21. Yuan, F.; Wang, Z.; Yu, X.; Wei, Z.; Li, S.; Wang, J.; Wang, S., Visualization of the Formation of Interfacially Polymerized Film by an Optical Contact Angle Measuring Device. *J. Phys. Chem. C* **2012,** *116*, (21), 11496-11506.
22. Vanhook, S. J.; Schatz, M. F.; Swift, J. B.; McCormick, W. D.; Swinney, H. L., Long-wavelength surface-tension-driven Benard convection: experiment and theory. *J. Fluid Mech.* **1997,** *345*, 45-78.
23. Karan, S.; Jiang, Z. W.; Livingston, A. G., Sub-10 nm polyamide nanofilms with ultrafast solvent transport for molecular separation. *Science* **2015,** *348*, (6241), 1347-1351.
24. Ma, X.-H.; Yao, Z.-K.; Yang, Z.; Guo, H.; Xu, Z.-L.; Tang, C. Y.; Elimelech, M., Nanofoaming of Polyamide Desalination Membranes To Tune Permeability and Selectivity. *Environ. Sci. Technol. Lett.* **2018,** *5*, (2), 123-130.
25. Ma, X.; Yang, Z.; Yao, Z.; Guo, H.; Xu, Z.; Tang, C. Y., Tuning roughness features of thin film composite polyamide membranes for simultaneously enhanced permeability, selectivity and anti-fouling performance. *J. Colloid Interface Sci.* **2019,** *540*, 382-388.
26. Song, X.; Gan, B.; Yang, Z.; Tang, C. Y.; Gao, C., Confined nanobubbles shape the surface roughness structures of thin film composite polyamide desalination membranes. *J. Membr. Sci.* **2019,** *582*, 342-349.
27. Liu, M.; Yu, S.; Tao, J.; Gao, C., Preparation, structure characteristics and separation properties of thin-film composite polyamide-urethane seawater reverse osmosis membrane. *J. Membr. Sci.* **2008,** *325*, (2), 947-956.
28. Donose, B. C.; Sukumar, S.; Pidou, M.; Poussade, Y.; Keller, J.; Gernjak, W., Effect of pH on the ageing of reverse osmosis membranes upon exposure to hypochlorite. *Desalination* **2013,** *309*, 97-105.
29. Wang, J.; Mo, Y.; Mahendra, S.; Hoek, E. M. V., Effects of water chemistry on structure and performance of polyamide composite membranes. *J. Membr. Sci.* **2014,** *452*, 415-425.
30. Stumm, W.; Morgan, J. J., *Aquatic chemistry: chemical equilibria and rates in natural waters*. John Wiley & Sons: 2012; Vol. 126.
31. Yao, Z.; Guo, H.; Yang, Z.; Qing, W.; Tang, C. Y., Preparation of nanocavity-contained thin film composite nanofiltration membranes with enhanced permeability and divalent to monovalent ion selectivity. *Desalination* **2018,** *445*, 115-122.
32. Ma, X.-H.; Yang, Z.; Yao, Z.-K.; Guo, H.; Xu, Z.-L.; Tang, C. Y., Interfacial Polymerization with Electrosprayed Microdroplets: Toward Controllable and Ultrathin Polyamide Membranes. *Environ. Sci. Technol. Lett.* **2018,** *5*, (2), 117-122.
33. Fane, A.; Tang, C.; Wang, R., Membrane technology for water: microfiltration, ultrafiltration, nanofiltration, and reverse osmosis. *Treatise on water science* **2011**.
34. Walton, N. R. G., Electrical-Conductivity and Total Dissolved Solids - What Is Their Precise Relationship. *Desalination* **1989,** *72*, (3), 275-292.
35. Guo, H.; Deng, Y.; Tao, Z.; Yao, Z.; Wang, J.; Lin, C.; Zhang, T.; Zhu, B.; Tang, C. Y., Does Hydrophilic Polydopamine Coating Enhance Membrane Rejection of Hydrophobic Endocrine-Disrupting Compounds? *Environ. Sci. Technol. Lett.* **2016,** *3*, (9), 332-338.
36. Yang, Z.; Guo, H.; Yao, Z. K.; Mei, Y.; Tang, C. Y., Hydrophilic Silver Nanoparticles Induce Selective Nanochannels in Thin Film Nanocomposite Polyamide Membranes. *Environ. Sci. Technol.* **2019,** *53*, (9), 5301-5308.

37. Idil Mouhoumed, E.; Szymczyk, A.; Schäfer, A.; Paugam, L.; La, Y. H., Physico-chemical characterization of polyamide NF/RO membranes: Insight from streaming current measurements. *J. Membr. Sci.* **2014,** *461*, 130-138.
38. Tang, C. Y. Y.; Kwon, Y. N.; Leckie, J. O., Effect of membrane chemistry and coating layer on physiochemical properties of thin film composite polyamide RO and NF membranes I. FTIR and XPS characterization of polyamide and coating layer chemistry. *Desalination* **2009,** *242*, (1-3), 149-167.
39. Hermans, S.; Bernstein, R.; Volodin, A.; Vankelecom, I. F. J., Study of synthesis parameters and active layer morphology of interfacially polymerized polyamide–polysulfone membranes. *React. Funct. Polym.* **2015,** *86*, 199-208.
40. Petersen, R. J., Composite Reverse-Osmosis and Nanofiltration Membranes. *J. Membr. Sci.* **1993,** *83*, (1), 81-150.
41. Tan, Z.; Chen, S. F.; Peng, X. S.; Zhang, L.; Gao, C. J., Polyamide membranes with nanoscale Turing structures for water purification. *Science* **2018,** *360*, (6388), 518-521.
42. Yu, S.; Liu, M.; Lü, Z.; Zhou, Y.; Gao, C., Aromatic-cycloaliphatic polyamide thin-film composite membrane with improved chlorine resistance prepared from m-phenylenediamine-4-methyl and cyclohexane-1,3,5-tricarbonyl chloride. *J. Membr. Sci.* **2009,** *344*, (1-2), 155-164.
43. Cumbal, L.; Sengupta, A. K., Arsenic removal using polymer-supported hydrated iron(III) oxide nanoparticles: Role of Donnan membrane effect. *Environ. Sci. Technol.* **2005,** *39*, (17), 6508-6515.
44. Oo, M. H.; Song, L. F., Effect of pH and ionic strength on boron removal by RO membranes. *Desalination* **2009,** *246*, (1-3), 605-612.
45. Do, V. T.; Tang, C. Y.; Reinhard, M.; Leckie, J. O., Effects of chlorine exposure conditions on physiochemical properties and performance of a polyamide membrane--mechanisms and implications. *Environ. Sci. Technol.* **2012,** *46*, (24), 13184-92.
46. Bernstein, R.; Belfer, S.; Freger, V., Toward Improved Boron Removal in RO by Membrane Modification: Feasibility and Challenges. *Environ. Sci. Technol.* **2011,** *45*, (8), 3613-3620.
47. Kanel, S. R.; Manning, B.; Charlet, L.; Choi, H., Removal of arsenic(III) from groundwater by nanoscale zero-valent iron. *Environ. Sci. Technol.* **2005,** *39*, (5), 1291-1298.
48. He, Y. R.; Tang, Y. P.; Ma, D. C.; Chung, T. S., UiO-66 incorporated thin-film nanocomposite membranes for efficient selenium and arsenic removal. *J. Membr. Sci.* **2017,** *541*, 262-270.
49. Guo, H.; Peng, L. E.; Yao, Z. K.; Yang, Z.; Ma, X. H.; Tang, C. Y. Y., Non-Polyamide Based Nanofiltration Membranes Using Green Metal-Organic Coordination Complexes: Implications for the Removal of Trace Organic Contaminants. *Environ. Sci. Technol.* **2019,** *53*, (5), 2688-2694.
50. Fujioka, T.; Kodamatani, H.; Nghiem, L. D.; Shintani, T., Transport of N-Nitrosamines through a Reverse Osmosis Membrane: Role of Molecular Size and Nitrogen Atoms. *Environ. Sci. Technol. Lett.* **2019,** *6*, (1), 44-48.